Author(s): Lehikoinen, Antti & Arkkio, Antero & Belahcen, Anouar

Title: Reduced basis finite element modelling of electrical machines with multi-conductor windings

Year: 2016

Version: Post print

Please cite the original version:

Lehikoinen, Antti & Arkkio, Antero & Belahcen, Anouar. 2016. Reduced basis finite element modelling of electrical machines with multi-conductor windings. International Conference on Electrical Machines. 7. 978-1-5090-2538-1 (electronic). DOI: 10.1109/icelmach.2016.7732918.

Reduced Basis Finite Element Modelling of Electrical Machines with Multi-Conductor Windings

Antti Lehikoinen, Antero Arkkio and Anouar Belahcen

***Abstract*—Finite element analysis of electrical machines with multi-conductor windings can be computationally costly. This paper proposes a solution to this problem, using a reduced basis approach. The field-circuit problem is first solved in a single slot only, with a set of different boundary conditions. These pre-computed solutions are then used as shape functions to approximate the solution in all slots of the full problem. A polynomial interpolation method is also proposed for coupling the slot domains with the rest of the geometry, even if the geometries or meshes do not fully conform on the boundary.**

The method is evaluated on several test problems. According to the simulations, accurate solutions are obtained. Furthermore, a speed-up factor of 30 is observed when analysing a six-slot phase belt of a high-speed induction machine.

***Index Terms*—Finite element analysis, eddy currents, proximity effects, reduced order systems.**

I. Introduction

The prevailing efficiency and performance demands require an accurate prediction of resistive losses in the windings of an electrical machine. Outside very simple geometries, finite element (FE) analysis is typically required due to the eddy-current phenomena. However, this can be a computationally formidable task due to the dense mesh required, especially if the number of conductors is large. This is true especially at higher frequencies, e.g. when considering the effect of voltage harmonics from converter supply.

These high-frequency resistive losses can be divided into skin- and proximity-effect losses – the latter of which is typically dominant – and circulating currents. The former two are related to the uneven current density distribution *within a conductor*, whereas the latter refers to the uneven distribution of total current *between conductors* connected in parallel. Modelling both phenomena requires taking into account the conductor-level field solution as well as the total winding configuration.

Proximity effects have been often analysed by time- or frequency-domain homogenization [1]–[8]. However, these studies have mostly focused on purely series-connected coils, or idealized Litz wires. By contrast, the scarce research on circulating currents has mostly ignored the proximity effects [9]–[12]. Some brute-force and analytical approaches have also been studied, typically with problems with relatively few conductors [13]–[21].

This paper proposes a reduced basis approach for analysing both the proximity and circulating current effects in a computationally efficient fashion. The method has been heavily inspired by the recently-proposed domain decomposition approach [22], but addresses many of its drawbacks related to analysing electrical machines in particular. Indeed, the proposed method can be directly applied on arbitrary and uneven conductor packings inside a slot of any shape. Furthermore, a nonconforming coupling is proposed between the domains, allowing for easy handling of curved boundaries and a great liberty for meshing. Finally, the online computation cost should be significantly lower for the proposed method, although this remains to be verified.

The accuracy and efficiency of the method are then evaluated on several demonstrative problems. A high-speed induction machine is used as an example, with the focus on the supply voltage harmonics. According to the simulations, the method is sufficiently accurate and yields significant computational time savings in realistic problems. Thus, it could be very useful in the design and optimization of high-performance electrical machines.

II. Reduced Basis Approach

This paper proposes an approach for 2D field-circuit FE analysis of an electrical machine with a large number of conductors per stator slot. Using traditional techniques, this type of analysis would be computationally costly due to the large number of degrees-of-freedom (DoF) required for each slot. In the proposed method, a set of solutions is first computed for one slot and different boundary conditions. These solutions are then used as shape functions in the full problem, to approximate the solution in all slots of the machine. On the slot boundary, they are coupled together with the typical nodal-based shape functions. The method will be referred to as a reduced-basis approach due to the use of pre-computed solutions. However, it obviously bears a close resemblance to domain decomposition methods as well.

Throughout this paper, the following terms are adopted. The slot domain with the pre-computed solutions is referred

The research leading to these results has received funding from the European Research Council under the European Unions Seventh Framework Programme (FP7/2007-2013) / ERC Grant Agreement n. 339380.

A. Lehikoinen, A. Arkkio and A. Belahcen are with Aalto University, Dept. of Electrical Engineering and Automation, P.O. Box 13000, FI-00076 Espoo, Finland. (e-mail: antti.lehikoinen@aalto.fi, antero.arkkio@aalto.fi, anouar.belahcen@aalto.fi).

A. Belahcen is also with Tallinn University of Technology, 19086 Tallinn, Estonia.

to as the *reduced domain*, whereas the rest of the machine excluding the slots is called *main domain*. Similar terminology is used for the meshes. The term *main problem* shall refer to analysing the full problem domain with the proposed method. The tilde notation $\tilde{\mathbf{a}}$ will be used for reduced domain quantities. Furthermore, a *coupling boundary* will be defined to couple the domains together, the shape of which is defined by *coupling nodes*. In the general case, this coupling boundary does not need to conform exactly to the boundaries of either the main or reduced domains.

A slightly similar domain decomposition approach with Dirichlet-to-Neumann mapping (DtN) was presented in [22]. This DtN method was based on a regular tessellation of a winding, with one hexagonal tile per conductor. However, this approach would be difficult to apply to more complex slot shapes with a non-uniform packing of conductors. Thus, in this paper the entire slot is modelled at once. The computation cost for the reduced domain is of course higher, but should not be intolerable with typical slot shapes and realistic mesh densities. Additionally, using the DtN method on the uneven packing would probably require solving several reduced domain problems with different tile shapes, increasing both the solution and overhead times.

Furthermore, the DtN method required a conforming meshing at the boundary between main and reduced domains. By contrast, the proposed method allows for discrepancies between the meshes and even the geometries themselves. Finally, the DtN method had a minimum of 2 DoFs per conductor in the main domain analysis, whereas the proposed method has DoFs only on the coupling boundary. Indeed, in the examples good results shall be seen with only 60 DoFs, where the DtN method would have required at least 672.

The analysis in this paper is limited to linear time-harmonic problems with first-order meshes and shape functions. However, extension to nonlinear problems and higher order discretization should be straightforward, and will be considered in future work. Problems in the time-domain might be more problematic, but should be feasible [22].

A. A-V Formulation

In this paper, the well-known A-V formulation is used, so the solution of the Galerkin-discretized field-circuit problem consists of the vector potential $\mathbf{a}$, voltages $\mathbf{u}$ over the conductors and a set of linearly independent currents (typically loop currents) $\mathbf{i}$ [23]. Thus the problem can be expressed as

$$\begin{bmatrix} \mathbf{Q} & \mathbf{C}_\mathrm{J} & \mathbf{0} \\ \mathrm{j}\omega\mathbf{C}_\mathrm{E} & -\mathbf{I} & \mathbf{RL} \\ \mathbf{0} & \mathbf{L}^\mathrm{T} & \mathbf{Z} \end{bmatrix} \begin{bmatrix} \mathbf{a} \\ \mathbf{u} \\ \mathbf{i} \end{bmatrix} = \begin{bmatrix} \mathbf{0} \\ \mathbf{0} \\ \mathbf{u}_\mathrm{s} \end{bmatrix}, \tag{1}$$

where $\mathbf{Q} = \mathbf{S} + \mathrm{j}\omega\mathbf{M}$ is the well-known stiffness-mass matrix. The matrices $\mathbf{C}_\mathrm{J}$ and $\mathbf{C}_\mathrm{E}$ with the entries

$$[\mathbf{C}_\mathrm{J}]_{ij} = \frac{-\sigma}{l_\mathrm{e}} \int_{\Omega_j^\mathrm{c}} \varphi_i \mathrm{d}S \tag{2}$$

$$[\mathbf{C}_\mathrm{E}]_{ij} = R_i \int_{\Omega_i^\mathrm{c}} \varphi_j \mathrm{d}S \tag{3}$$

describe the current density in the conductors due to the voltages $\mathbf{u}$, and the back-emfs induced on the conductors, respectively. The conductivity and axial length are denoted by σ and l_e, and Ω and Ω_i^c are the entire problem domain, and the domain of the conductor i. Finally, $\mathbf{R}$ is a diagonal matrix of the conductor resistances R_i, $\mathbf{Z}$ is the end-winding impedance, and $\mathbf{L}$ is the loop matrix describing the winding connection, with the entries

$$[\mathbf{L}]_{ij} = \begin{cases} 1 & \text{current } j \text{ flows through conductor } i \text{ forwards} \\ -1 & \text{current } j \text{ flows through conductor } i \text{ backwards} \\ 0 & \text{otherwise.} \end{cases} \tag{4}$$

B. Solution on the Reduced Domain

Now, only a single slot of the machine is considered, on the domain Ω^s with N_c conductors. Within the slot, the reduced-domain $\tilde{\mathbf{a}}$ and $\tilde{\mathbf{u}}$ are fully determined by the currents $\tilde{\mathbf{i}}$ flowing in the conductors, and the boundary values of the vector potential on the boundary $\partial\Omega^\mathrm{s}$. For generality, all conductors are assumed to be parallel-connected, so $\tilde{\mathbf{u}}$ and $\tilde{\mathbf{i}}$ have the same size. Due to the absence of iron components, the problem can be assumed linear.

Indeed, the solution of this discrete problem is spanned by a finite number of boundary data. Firstly, let $n_1, n_2, \ldots, n_{N^\mathrm{bnd}}$ be the boundary nodes of some meshing for Ω^s, and $\partial\tilde{\mathbf{a}}$ denote the nodal potentials on the boundary. Next, a set of solutions is computed

$$\mathbf{X}^\mathrm{A} = \begin{bmatrix} \mathbf{x}_1^\mathrm{A} & \mathbf{x}_2^\mathrm{A} & \ldots & \mathbf{x}_{N^\mathrm{bnd}}^\mathrm{A} \end{bmatrix}, \tag{5}$$

with each solution

$$\mathbf{x}_k^\mathrm{A} = \begin{bmatrix} \tilde{\mathbf{a}}_k^\mathrm{A} \\ \tilde{\mathbf{u}}_k^\mathrm{A} \end{bmatrix} \tag{6}$$

corresponding to the following boundary data

$$\partial\tilde{\mathbf{a}}_k = \begin{cases} 1 & \text{at } n_k \\ 0 & \text{elsewhere} \end{cases}$$
$$\tilde{\mathbf{i}} = \mathbf{0}. \tag{7}$$

Likewise, another set of solutions is computed

$$\mathbf{X}^\mathrm{I} = \begin{bmatrix} \mathbf{x}_1^\mathrm{I} & \mathbf{x}_2^\mathrm{I} & \ldots & \mathbf{x}_{N_\mathrm{c}}^\mathrm{I} \end{bmatrix} \tag{8}$$

for the unit current sources

$$\partial\tilde{\mathbf{a}} = \mathbf{0}$$
$$\left[\tilde{\mathbf{i}}_k\right]_i = \begin{cases} 1 & i = k \\ 0 & i \neq k. \end{cases} \tag{9}$$

Both $\mathbf{X}^\mathrm{A}$ and $\mathbf{X}^\mathrm{I}$ can be easily obtained based on (1) by solving problems of type

$$\begin{bmatrix} \tilde{\mathbf{Q}} & \tilde{\mathbf{C}}_\mathrm{J} \\ \mathrm{j}\omega\tilde{\mathbf{C}}_\mathrm{E} & -\mathbf{I} \end{bmatrix} \mathbf{x} = \begin{bmatrix} -\mathbf{Q}_\mathrm{bnd}\partial\mathbf{a} \\ -\tilde{\mathbf{R}}\mathbf{i} \end{bmatrix}, \tag{10}$$

where $\mathbf{Q}_\mathrm{bnd}$ is the stiffness-mass matrix related to the non-zero Dirichlet boundary condition.

Now, the discretized solution on Ω^{s} for any arbitrary combination of currents $\tilde{\mathbf{i}}$ and boundary potential $\partial\tilde{\mathbf{a}}$ can be expressed as a linear combination of $\mathbf{X}^{\mathrm{A}}$ and $\mathbf{X}^{\mathrm{I}}$ as

$$\begin{bmatrix}\tilde{\mathbf{a}}\\ \tilde{\mathbf{u}}\end{bmatrix} = \begin{bmatrix}\mathbf{X}^{\mathrm{A}} & \mathbf{X}^{\mathrm{I}}\end{bmatrix}\begin{bmatrix}\partial\tilde{\mathbf{a}}\\ \tilde{\mathbf{i}}\end{bmatrix}. \tag{11}$$

Indeed, this solution is exactly the same (within numerical accuracy) as would be obtained by explicitly solving (10) with the same boundary data.

C. Boundary Interpolation

However, due to meshing requirements the number of boundary nodes N^{bnd} will usually be much larger than would be necessary to reasonably approximate any realistic boundary values $\partial\mathbf{a}$. Therefore, obtaining $\mathbf{X}^{\mathrm{A}}$ would present a large, mostly unnecessary computational burden. Thus, the isoparametric FE approach of order p is utilized here.

The coupling boundary C approximating $\partial\Omega^{\mathrm{s}}$ is defined as follows. A total $N^{\mathrm{cpl}} < N^{\mathrm{bnd}}$ coupling nodes located at $\hat{\mathbf{x}}_1, \ldots, \hat{\mathbf{x}}_{N^{\mathrm{cpl}}}$ are defined, with the $\hat{\mathbf{x}}$ falling on or near $\partial\Omega^{\mathrm{s}}$. A set of N^{cpl}/p (possibly curved) edges is defined to connect these nodes, with $p+1$ points on each edge and each end-point shared with the adjacent edge. Next, a 1D reference edge is defined with $p+1$ nodes $\hat{t}_i$ equally distributed on $[0,1]$, so that it is easy to define a set of polynomial shape functions $\hat{\psi}$ satisfying

$$\hat{\psi}_k(t) = \begin{cases} 1 & t = \hat{t}_k \\ 0 & t = \hat{t}_i, \quad i \neq k. \end{cases} \tag{12}$$

Then, each global edge e is defined by

$$\mathbf{x} = \sum_{k=1}^{p+1} \hat{\mathbf{x}}_{n_k^e}\hat{\psi}_k(t), \quad t \in [0,1], \tag{13}$$

where $\hat{\mathbf{x}}_{n_k^e}$ are the $p+1$ nodes belonging the edge. The final approximation C of $\partial\Omega^{\mathrm{s}}$ is then the union of these edges.

The boundary values $\partial\tilde{\mathbf{a}}$ can then be defined as a linear combination of a new set of N^{cpl} independent vector potential values $\partial\hat{\mathbf{a}}$ as follows. For each boundary node n_i of the meshing for Ω^{s}, the closest point on C is determined. If this point falls on the edge e with the corresponding reference coordinate t_i, the boundary potential is set to

$$[\partial\tilde{\mathbf{a}}]_i = \sum_{k=1}^{p+1} [\partial\hat{\mathbf{a}}]_{n_k^e}\hat{\psi}_k(t_i). \tag{14}$$

In practice, the closest point on C can be easily obtained by minimizing the distance with a few iterations of the Newton's method. The initial guess can be explicitly obtained by using a linear approximation of each edge with their end nodes only, and finding the closest point on that line segment.

The constant coefficients $\hat{\psi}_k(t_i)$ are then collected to a matrix $\mathbf{P}_{\mathrm{cr}}$, so that the relationship between $\partial\tilde{\mathbf{a}}$ and $\partial\hat{\mathbf{a}}$ can be compactly expressed as

$$\partial\tilde{\mathbf{a}} = \mathbf{P}_{\mathrm{cr}}\partial\hat{\mathbf{a}}. \tag{15}$$

Now, it is sufficient to compute $\mathbf{X}^{\mathrm{A}}$ for different $\partial\hat{\mathbf{a}}$ only.

The approach is illustrated in Fig. 1(a), in which a second-order edge (blue) is used to approximate a quarter-circle slot bottom half (black). The end-nodes of the edge are plotted with the circles, while a dot is used for the center node. As can be seen, even this coarse approximation matches the boundary shape relatively well. The shape function values associated with the center node (red) and end node (blue) of the edge are also shown in Fig 1(b).

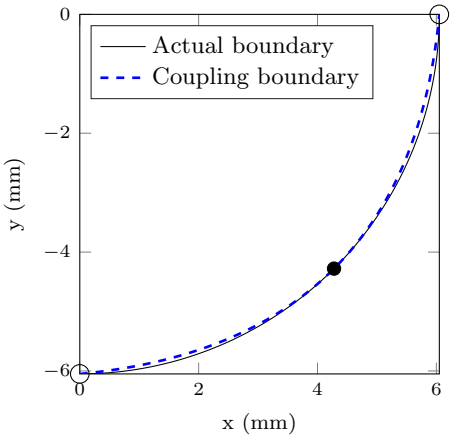

(a) A circular boundary approximated with a second-order coupling boundary.

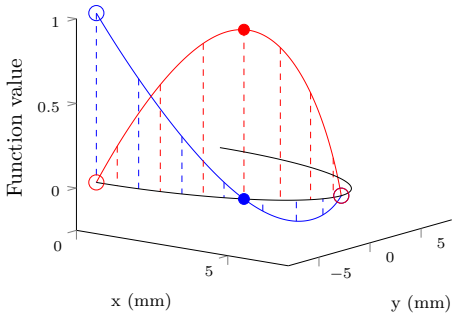

(b) Boundary shape functions.

Fig. 1. Illustration of the isoparametric coupling boundary.

D. Coupling

Now, the remaining task is to utilize the slot solutions for obtaining the solution for entire domain Ω in an efficient fashion. The case with only one slot is considered for clarity, assuming only the reduced domain has conducting parts. The discrete problem can then be written as

$$\begin{aligned} \mathbf{S}\mathbf{a} &= 0 \\ \tilde{\mathbf{Q}}\tilde{\mathbf{a}} + \tilde{\mathbf{C}}_{\mathrm{J}}\tilde{\mathbf{u}} &= 0 \\ \mathbf{L}^{\mathrm{T}}\tilde{\mathbf{u}} + \mathbf{Z}\tilde{\mathbf{i}} &= \mathbf{u}_{\mathrm{s}}, \end{aligned} \tag{16}$$

where the first equation governs the main domain. By writing $\mathbf{a}_{\mathrm{r}}$ and $\mathbf{u}_{\mathrm{r}}$ with (11) and redefining the test-function side as

$\mathbf{a}^{\mathrm{A}}$, the latter two equations can be re-written as

$$\hat{\mathbf{R}}_{\mathrm{AA}}\partial\hat{\mathbf{a}} + \hat{\mathbf{R}}_{\mathrm{AI}}\mathbf{L}\tilde{\mathbf{i}} = 0$$
$$\mathbf{L}^{\mathrm{T}}\hat{\mathbf{R}}_{\mathrm{UA}}\partial\hat{\mathbf{a}} + \mathbf{L}^{\mathrm{T}}\hat{\mathbf{R}}_{\mathrm{UI}}\mathbf{L}\tilde{\mathbf{i}} + \mathbf{Z}\tilde{\mathbf{i}} = \mathbf{u}_{\mathrm{s}} \quad (17)$$

with the newly-introduced reduced matrices

$$\hat{\mathbf{R}}_{\mathrm{AA}} = (\tilde{\mathbf{a}}^{\mathrm{A}})^{\mathrm{T}}\tilde{\mathbf{Q}}\tilde{\mathbf{a}}^{\mathrm{A}} + (\tilde{\mathbf{a}}^{\mathrm{A}})^{\mathrm{T}}\tilde{\mathbf{C}}_{\mathrm{J}}\tilde{\mathbf{u}}^{\mathrm{A}} \quad (18)$$
$$\hat{\mathbf{R}}_{\mathrm{AI}} = (\tilde{\mathbf{a}}^{\mathrm{A}})^{\mathrm{T}}\tilde{\mathbf{Q}}\tilde{\mathbf{a}}^{\mathrm{I}} + (\tilde{\mathbf{a}}^{\mathrm{A}})^{\mathrm{T}}\tilde{\mathbf{C}}_{\mathrm{J}}\tilde{\mathbf{u}}^{\mathrm{I}} \quad (19)$$
$$\hat{\mathbf{R}}_{\mathrm{UA}} = \tilde{\mathbf{u}}^{\mathrm{A}} \quad (20)$$
$$\hat{\mathbf{R}}_{\mathrm{UI}} = \tilde{\mathbf{u}}^{\mathrm{I}}. \quad (21)$$

Indeed, the solution of the main problem only consists of $\mathbf{a}$ for representing the main domain solution, and $\partial\hat{\mathbf{a}}$ and $\tilde{\mathbf{i}}$ for representing the reduced domain solution.

Finally, the main and reduced domains have to be coupled together at the slot boundary. In this paper, $\partial\hat{\mathbf{a}}$ are retained as independent variables, and the boundary potentials of the main domain are interpolated as $\partial\mathbf{a} = \mathbf{P}_{\mathrm{cm}}\partial\hat{\mathbf{a}}$ and eliminated. The interpolation matrix $\mathbf{P}_{\mathrm{cm}}$ can be obtained with the same procedure as described in (12)-(15).

Obviously, the coupling nodes could also be slaved to the main domain instead of vice versa. However, it is a common practice to use the higher-reluctivity side of the boundary as the master variable, in e.g. the mortar element method. Furthermore, in the computation examples it shall be seen that using a larger number of coupling nodes can increase accuracy even with a coarse main mesh.

This approach allows for a great freedom in representing the main domain. Curved boundaries can be approximated very coarsely if desired, i.e. the geometry itself can be nonconforming with both the reduced domain and the coupling boundary. Even with a fully conforming geometry, the main mesh nodes do not have to coincide with the coupling nodes. This is a great benefit with many meshing tools, in which specifying boundary nodes is difficult. Furthermore, the density of coupling nodes can be adjusted freely based on the assumed smoothness of the solution on the boundary.

III. Simulations

A hypothetical high-speed machine with two parallel paths and 56 subconductors per path is used as a demonstrative problem. The main dimensions of the machine can be found in Table I. The rotor of the machine is ignored, since analysing a solid conducting rotor would present a significant computational cost in itself and could thus confound the computational time analysis. The simulations were performed with Matlab on a 3.2 GHz 8-core computer.

A. Single Trapezoidal Slot

A single slot segment the with a trapezoidal slot shape shown in Fig. 2 was analysed first. The slot domain used in the proposed reduced basis approach is marked with blue. There were a total of 336 strands in the slot, plotted in red in the Fig. The supply frequency was 6050 Hz, corresponding to the 11th harmonic of the fundamental often present in pulse-amplitude modulation. The winding connection was set to correspond to the first slot of the machine, i.e. with phases (a) and -(c).

TABLE I
Main Dimensions of the Machine.

Winding connection	Delta
Number of parallel paths	2
Number of winding layers	2
Number of turns	3
Number of strands per slot	336
Number of stator slots	36
Coil pitch (slots)	12
Stator diameter (mm)	288

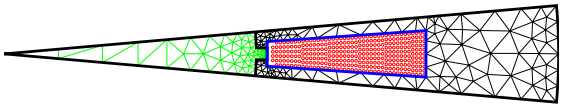

Fig. 2. A stator slot segment with a trapezoidal slot. The coarsest main mesh is also shown. Air domain is plotted in green, whereas the reduced domain is highlighted in blue.

The reduced domain was meshed with two layers of elements per strand, resulting in 21789 nodal DoFs. For a reference solution, a brute-force simulation was performed with the entire segment densely meshed with 153405 DoFs, taking 2.7 seconds to solve. A part of the reduced domain mesh near the slot bottom corner has been illustrated in Fig. 3.

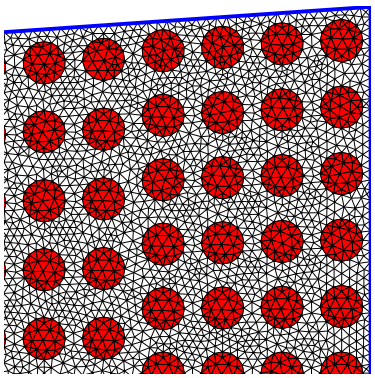

Fig. 3. A part of the reduced domain mesh. Strands have been highlighted in red.

The fully conforming case was analysed first, i.e. with the coupling nodes coinciding with the main mesh nodes. The initial coarse discretization shown in Figure 2 resulted in 141 nodes in the mesh, of which 30 were coupling nodes. The iron part of the mesh was later uniformly refined and the simulations were repeated.

The results are shown in Table II. Shown are the number of coupling nodes, the relative errors $||\mathbf{i} - \mathbf{i}_{\mathrm{ref}}||/||\mathbf{i}_{\mathrm{ref}}||$, $||\mathbf{P} - \mathbf{P}_{\mathrm{ref}}||/||\mathbf{P}_{\mathrm{ref}}||$ between the vectors of currents and the per-conductor total losses, and the time needed for computing

the reduced domain solutions. Unsurprisingly, refining the mesh improved accuracy.

The simulations were repeated for a non-conforming case, with the coupling nodes defined independently from either mesh and spaced approximately uniformly on the boundary. Both first- and second-order coupling boundaries were analysed, and the results are shown in Table III. It can be seen that with 30 nodes, the errors are roughly 50% smaller than in the conforming case with 37. This can be probably mainly be attributed to the distribution of coupling nodes: the nonconforming approach had a larger portion of the coupling on the slot sides where $\mathbf{a}$ exhibited sharp spatial changes due to the circulating currents. However, the order of boundary did not seem to have any consistent effect on accuracy.

With the pre-computed reduced solutions, the main problem could be solved in approximately 2 milliseconds in each case. Obviously, in this simple example this benefit is completely offset by the long initialization times compared to the brute-force approach. However, the proposed method appears reasonably accurate. Furthermore, in a non-linear problem the reduced approach might outperform the brute-force one even in this case, assuming the convergence of the reduced solution is not extremely poor.

TABLE II
CONFORMING COUPLING BETWEEN DOMAINS.

No. of coupling nodes	$\mathbf{i}$ error (%)	$\mathbf{P}$ error (%)	Initialization (s)
37	11.50	9.11	12.95
74	5.94	5.41	14.34
296	0.54	0.28	21.63

TABLE III
NON-CONFORMING COUPLING BETWEEN DOMAINS.

No. of coupling nodes	Bnd. Order	$\mathbf{i}$ error (%)	$\mathbf{P}$ error (%)
33	1	6.31	5.58
62	1	1.17	0.87
62	2	1.10	0.85
112	1	0.632	0.352
112	2	0.648	0.362

B. Single Smooth Slot

The method was then evaluated on a more difficult problem. The frequency was increased to 50 kHz, often used as switching frequency in pulse-width modulation. Furthermore, the slot shape was changed to a rounded one seen in Fig. 4.

In the previous example, the domain boundaries consisted of a few linear segments. Thus, the actual geometries of the main and reduced domain conformed to each other at the boundary, even though the coupling nodes and the main mesh nodes did not. As can be seen from the close-ups in Fig. 5, this is no longer the case. Furthermore, refining the main mesh has a direct effect on this level of nonconformity, visible in the right subfigure.

Two types of approaches were evaluated. Table IV shows the results with coupling boundary conforming to the main domain, and the Dirichlet nodes matching the boundary nodes of the main mesh. By contrast, in Table V the coupling boundary conforms approximately to the reduced domain, and the Dirichlet nodes are spaced approximately equally on the boundary. In the latter case, only the coarsest main mesh is utilized.

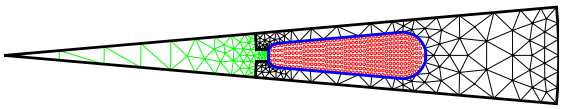

Fig. 4. A stator slot segment with a rounded slot. The coarsest main mesh also shown.

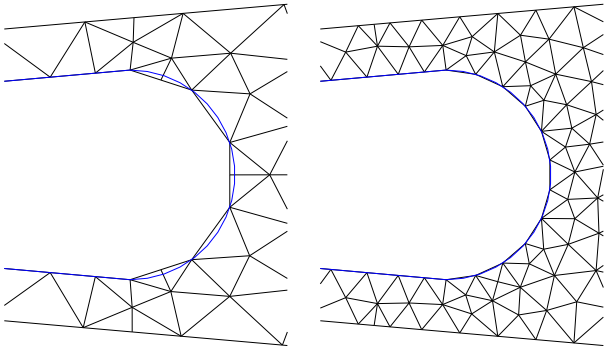

(a) (b)

Fig. 5. Main meshes of two different refinement levels. The boundary of the reduced domain has been highlighted in blue.

Once again, the latter approach fares better. Furthermore, in this case using a second-order boundary seems to yield a small but consistent improvement in accurary. This is most likely explained by the ability of the nonlinear boundary to better approximate the curved geometry with a smaller number of coupling nodes. Indeed, the last two simulations with the highest number of nodes are approximately on par. Furthermore, a deeper examination of the results revealed that the vector potential behaved relatively smoothly on the curved boundaries. Thus, further differences in favour of higher-order boundaries could probably be expected in problems where this is not the case.

TABLE IV
BOUNDARY CONFORMING TO THE MAIN DOMAIN.

No. of coupling nodes	$\mathbf{i}$ error (%)	$\mathbf{P}$ error (%)
41	13.19	10.62
75	5.49	4.58
116	4.44	4.61

As an example, Fig. 6 shows the distribution of total per-conductor losses in the slot. As Fig. 6(a) reveals, the largest losses can be found near the borders between winding turns, due to the circulating current effects [9]. The error in losses – compared to the reference solution – has been plotted in Fig. 6(b). The results are relatively accurate even conductor-by-conductor, even near the slot opening where the field distribution is probably the most complicated.

TABLE V
BOUNDARY CONFORMING TO THE REDUCED DOMAIN.

No. of coupling nodes	Bnd. Order	$\mathbf{i}$ error (%)	$\mathbf{P}$ error (%)
38	1	10.49	9.46
38	2	9.84	8.73
60	1	3.83	3.52
60	2	3.57	2.98
94	1	1.72	1.79
94	2	1.74	1.48

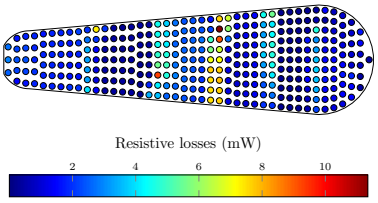

(a) Total losses.

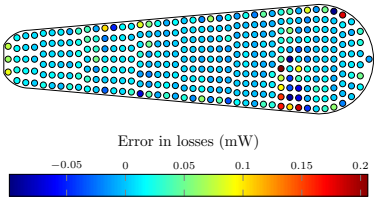

(b) Error in losses.

Fig. 6. Calculated resistive losses in the conductors.

C. Machine Sector

The simulations were repeated once more at 6050 Hz for one phase belt of the machine, i.e. a total of 6 slots. Using the same refinement level as before resulted in 1.1 million DoFs in the reference problem. Due to memory requirements, this problem could no longer be solved by direct methods with 8 GB of RAM. Thus, the ILU-preconditioned quasi-minimal residual method (QMR) was used, taking 216 iterations to converge. The total solution time was 412 seconds, plus the 54 seconds used on matrix assembly.

For the proposed method, the main mesh shown in Fig. 7 was used, with 921 DoFs. A total of four simulations were performed, with the coupling boundary approximately conforming to the reduced domain. As can be seen from Table VI, using a higher-order coupling boundary again appears beneficial when the number of coupling nodes is low.

TABLE VI
BOUNDARY CONFORMING TO THE REDUCED DOMAIN.

No. of coupling nodes	Bnd. Order	$\mathbf{i}$ error (%)	$\mathbf{P}$ error (%)
60	1	0.62	0.402
60	2	0.55	0.348
94	1	0.44	0.315
94	2	0.44	0.322

In this problem, the speed of the proposed method became evident. Indeed, calculating the reduced solutions required approximately 14-15 seconds in total, after which the main problem could be assembled and solved in less than 0.15 in each case, yielding a 30-fold speed advantage. The speed-up should be even larger in problems in which the main problem has to be solved several times without changing the reduced domain, such as nonlinear simulations or changing the supply voltage or even winding connection. The latter case would be e.g. Monte-Carlo analysis of circulating currents [9].

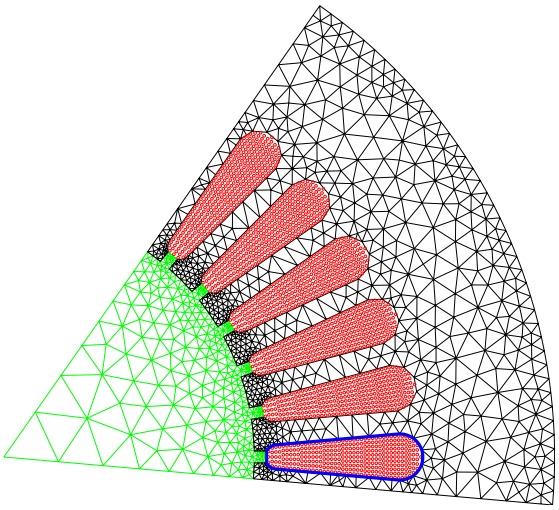

Fig. 7. The main mesh used for the phase belt simulation. The elementary reduced domain is highlighted with blue.

Due to scientific curiosity, the proposed method was used once more to simulate the entire cross-section of the machine. Obviously, no reference solution was available at this time, so the accuracy could not be evaluated. However, the method was once again very fast, taking only 0.5 seconds more time than in the phase belt simulation.

IV. CONCLUSION

A method was proposed for efficient finite element computation of resistive losses in the windings of electrical machines. The field-circuit problem was first solved in a single slot with different boundary conditions. These solutions were then used as basis functions in all slots of the machine, and coupled together with the traditional nodal shape functions on the boundary. For this coupling, an isoparametric approach was proposed, allowing for easy handling of nonconformity on the mesh or even geometry level.

The method was then evaluated on a high-speed induction machine, with the focus on supply harmonics. According to the simulations, the method yields reasonably accurate results, being significantly faster than the brute-force approach in realistic problems. Furthermore, the proposed coupling method appears to handle curved boundaries and inter-domain nonconformity in a robust fashion. Thus, the method should be suitable for computationally efficient design and analysis of high-performance electrical machines.

Obviously, some further work is still needed. The method should be verified on a nonlinear problem as well. Additionally, the method should be extended to either time-domain or harmonic balance analysis.

REFERENCES

[1] J. Gyselinck and P. Dular, "Frequency-domain homogenization of bundles of wires in 2-D magnetodynamic FE calculations," *IEEE Trans. Magn.*, vol. 41, no. 5, pp. 1416–1419, May 2005.

[2] J. Gyselinck, P. Dular, N. Sadowski, P. Kuo-Peng, and R. Sabariego, "Homogenization of form-wound windings in frequency and time domain finite-element modeling of electrical machines," *IEEE Trans. Magn.*, vol. 46, no. 8, pp. 2852–2855, Aug 2010.

[3] R. Sabariego, P. Dular, and J. Gyselinck, "Time-domain homogenization of windings in 3-D finite element models," *IEEE Trans. Magn.*, vol. 44, no. 6, pp. 1302–1305, June 2008.

[4] J. Gyselinck, R. Sabariego, and P. Dular, "Time-domain homogenization of windings in 2-D finite element models," *IEEE Trans. Magn.*, vol. 43, no. 4, pp. 1297–1300, April 2007.

[5] Z. De Greve, O. Deblecker, J. Lobry, and J.-P. Keradec, "High-frequency multi-winding magnetic components: From numerical simulation to equivalent circuits with frequency-independent RL parameters," *IEEE Trans. Magn.*, vol. 50, no. 2, pp. 141–144, Feb 2014.

[6] J. Sibue, J. Ferrieux, G. Meunier, and R. Periot, "Modeling of losses and current density distribution in conductors of a large air-gap transformer using homogenization and 3-D FEM," *IEEE Trans. Magn.*, vol. 48, no. 2, pp. 763–766, Feb 2012.

[7] J.-R. Sibue, G. Meunier, J.-P. Ferrieux, J. Roudet, and R. Periot, "Modeling and computation of losses in conductors and magnetic cores of a large air gap transformer dedicated to contactless energy transfer," *IEEE Trans. Magn.*, vol. 49, no. 1, pp. 586–590, Jan 2013.

[8] X. Nan and C. Sullivan, "An equivalent complex permeability model for litz-wire windings," *IEEE Trans. Ind. Appl.*, vol. 45, no. 2, pp. 854–860, March 2009.

[9] A. Lehikoinen, N. Chiodetto, E. Lantto, A. Arkkio, and A. Belahcen, "Monte carlo analysis of circulating currents in random-wound electrical machines," *IEEE Trans. Magn.*, 2016, in press.

[10] A. Lehikoinen and A. Arkkio, "Efficient finite-element computation of circulating currents in thin parallel strands," *IEEE Trans. Magn.*, vol. 52, no. 3, pp. 1–4, March 2016.

[11] M. van der Geest, H. Polinder, J. Ferreira, and D. Zeilstra, "Current sharing analysis of parallel strands in low-voltage high-speed machines," *IEEE Trans. Ind. Electron.*, vol. 61, no. 6, pp. 3064–3070, June 2014.

[12] F. Jiancheng, L. Xiquan, B. Han, and K. Wang, "Analysis of circulating current loss for high-speed permanent magnet motor," *IEEE Trans. Magn.*, vol. 51, no. 1, pp. 1–13, Jan 2015.

[13] R. Wrobel, D. Staton, R. Lock, J. Booker, and D. Drury, "Winding design for minimum power loss and low-cost manufacture in application to fixed-speed PM generator," *IEEE Trans. Ind. Appl.*, vol. 51, no. 5, pp. 3773–3782, Sept 2015.

[14] M. Fujita, Y. Kabata, T. Tokumasu, K. Nagakura, M. Kakiuchi, and S. Nagano, "Circulating currents in stator coils of large turbine generators and loss reduction," *IEEE Trans. Ind. Appl.*, vol. 45, no. 2, pp. 685–693, March 2009.

[15] M. Islam, S. Mir, and T. Sebastian, "Effect of paralleling the stator coils in a permanent-magnet machine," *IEEE Trans. Ind. Appl.*, vol. 42, no. 6, pp. 1429–1436, Nov 2006.

[16] M. Vetuschi and F. Cupertino, "Minimization of proximity losses in electrical machines with tooth-wound coils," *IEEE Trans. Ind. Appl.*, vol. 51, no. 4, pp. 3068–3076, July 2015.

[17] A. Tessarolo, F. Agnolet, F. Luise, and M. Mezzarobba, "Use of time-harmonic finite-element analysis to compute stator winding eddy-current losses due to rotor motion in surface permanent-magnet machines," *IEEE Trans. Energy Convers.*, vol. 27, no. 3, pp. 670–679, Sept 2012.

[18] Y. Amara, P. Reghem, and G. Barakat, "Analytical prediction of eddy-current loss in armature windings of permanent magnet brushless ac machines," *IEEE Trans. Magn.*, vol. 46, no. 8, pp. 3481–3484, Aug 2010.

[19] L. J. Wu, Z. Q. Zhu, D. Staton, M. Popescu, and D. Hawkins, "Analytical model of eddy current loss in windings of permanent-magnet machines accounting for load," *IEEE Trans. Magn.*, vol. 48, no. 7, pp. 2138–2151, July 2012.

[20] S. Iwasaki, R. P. Deodhar, Y. Liu, A. Pride, Z. Q. Zhu, and J. J. Bremner, "Influence of pwm on the proximity loss in permanent-magnet brushless ac machines," *IEEE Trans. Ind. Appl.*, vol. 45, no. 4, pp. 1359–1367, July 2009.

[21] A. G. Sarigiannidis and A. G. Kladas, "Switching frequency impact on permanent magnet motors drive system for electric actuation applications," *IEEE Trans. Magn.*, vol. 51, no. 3, pp. 1–4, March 2015.

[22] L. Lehti, J. Keränen, S. Suuriniemi, and L. Kettunen, "Coil winding losses: Decomposition strategy," *IEEE Trans. Magn.*, vol. 52, no. 1, pp. 1–6, Jan 2016.

[23] I. A. Tsukerman, A. Konrad, and J. D. Lavers, "A method for circuit connections in time-dependent eddy current problems," *IEEE Trans. Magn.*, vol. 28, no. 2, pp. 1299–1302, Mar 1992.

V. BIOGRAPHIES

Antti Lehikoinen was born in December 1988. He received his Bachelor's degree in Science (tech) in 2012 from the Aalto University School of Electrical Engineering, and the M.Sc. degree a year later from the same institute, with a major in electromechanics.

He is currently pursuing his doctoral degree in the School of Electrical Engineering, Espoo, Finland. He is mainly focusing on efficient finite element modelling of the winding losses of electrical machines, and the stochastic properties of circulating current losses in random-wound machines.

Antero Arkkio was born in Vehkalahti, Finland in 1955. He received his M.Sc. (Tech.) and D.Sc. (Tech.) degrees from Helsinki University of Technology in 1980 and 1988. Currently he is a Professor of Electrical Engineering at Aalto University. His research interests deal with modeling, design, and measurement of electrical machines.

Anouar Belahcen (M13,SM15) was born in Morocco, in 1963. He received the B.Sc. degree in physics from the University Sidi Mohamed Ben Abdellah, Fes, Morocco, in 1988 and the M.Sc. (Tech.) and Doctor (Tech.) degrees from Helsinki University of Technology, Finland, in 1998, and 2004, respectively. From 2008 to 2013, he has been working as Adjunct Professor in the field of coupled problems and material modeling at Aalto University, Finland. Since 2011 he is Professor of electrical machines at Tallinn University of Technology, Estonia and in 2013 he became Professor of Energy and Power at Aalto University. His research interest are numerical modeling of electrical machines, especially magnetic material modeling, coupled magnetic and mechanical problems, magnetic forces, and magnetostriction.